

# Influence of heat-treatment on the sliding wear of thermal spray cermet coatings

V. Stoica<sup>a</sup>, R. Ahmed<sup>a,\*</sup>, T. Itsukaichi<sup>b</sup>

<sup>a</sup>*Mechanical Engineering, School of Engineering and Physical Sciences, Heriot Watt University, James Nasmyth Building, Edinburgh, EH14 4AS, United Kingdom*

<sup>b</sup>*Fujimi Incorporated, 82-28 Kakamihigashi-machi-5, Kakamigahara, Gifu, Japan*

Received 10 October 2003; accepted in revised form 21 March 2005

Available online 17 May 2005

## Abstract

Functionally graded WC–NiCrBSi coatings were thermally sprayed using a High Velocity Oxy-Fuel (JP5000) system and heat-treated at 1200 °C in argon environment. The relative performance of the as-sprayed and heat-treated coatings was investigated in sliding wear under different tribological conditions of contact stress, and test couple configuration, using a high frequency reciprocating ball on plate rig. Test results are discussed with the help of microstructural evaluations and mechanical properties measurements. Results indicate that by heat-treating the coatings at a temperature of 1200 °C, it is possible to achieve higher wear resistance, both in terms of coating wear, as well as the total wear of the test couples. This was attributed to the improvements in the coating microstructure during the heat-treatment, which resulted in an improvement in coating's mechanical properties through the formation of hard phases, elimination of brittle W<sub>2</sub>C and W, and the establishment of metallurgical bonding within the coating microstructure.

© 2005 Elsevier B.V. All rights reserved.

*Keywords:* Thermal spray coatings; Heat-treatment; Sliding wear; Microstructure; Mechanical properties

## 1. Introduction

The performance of thermally sprayed cermet coatings in wear applications is influenced primarily by the carbide size, volume fraction, and phase composition of the coatings. Tungsten carbide coupled with Co, CoCr, Ni or NiCrBSi matrix has been the preferred material for industrial applications used to reduce wear. This is due to the combined effect of the hardness of carbides and toughness of the metal matrix. Among the binder materials, Ni-based self fluxing alloy combines a number of special properties brought by its constituents, e.g. nickel brings excellent wettability which promotes good cohesion, chromium improves the tribo-mechanical properties, boron reduces the melting point, silicon increases self-fluxing properties, iron modifies the diffusion rates [1]. Their synergetic effect thus enhances the wear resistance of the coatings [2–4].

Latest solutions in HVOF thermal spraying technology, e.g. liquid fuel HVOF spraying, have been shown to produce dense coatings with minimum decarburisation, which exhibit superior wear resistance. However, problems associated with the partial melting of the particles causing poor bonding, both at the intersplat and coating substrate interface levels, are still encountered even with the state of the art HVOF liquid fuel systems. One way of improving the coating's performance is through the use of post-deposition heat-treatment, and several investigations over the last decade have established that microstructural changes associated with such heat-treatments can significantly improve the wear resistance of thermally sprayed cermet coatings [3,5–8]. Although the exact nature of coating material, heat-treatment and heat-treatment conditions, vary in the published literature, e.g. in terms of temperature range of 800 to 1200 °C, and the tribological evaluations, can not be directly compared, some structure property relationships have been established. Recently, the authors of this paper reported the results of sliding wear evaluations of the Hot Isostatically Pressed (HIPed) WC–

\* Corresponding author. Tel.: +44 131 4514722; fax: +44 131 4513129.

E-mail address: [R.Ahmed@hw.ac.uk](mailto:R.Ahmed@hw.ac.uk) (R. Ahmed).

NiCrBSi cermet coatings at temperatures of 850 to 1200 °C, where both temperatures were shown to significantly improve the sliding wear resistance of test couples [9]. The objective of the current investigation was thus to consider the influence of the heat-treatment method, i.e. heat-treatment as opposed to HIPing, at the higher temperature of 1200 °C. This research thus addresses the post-deposition heat-treatment, with an aim to comprehend the relative performance of the as-sprayed and heat-treated WC–NiCrBSiFeC coatings in sliding wear conditions, and relate it to the coating microstructure and mechanical properties.

## 2. Experimental procedure

### 2.1. Coating preparation

Two compositions of the spray dried and sintered WC–NiCrBSiFeC composite powders, i.e. 10 wt.% Ni alloy, 90 wt.% WC and 40 wt.% Ni alloy, 60 wt.% WC, were used in this investigation. The properties of these powders are listed in Table 1. The substrates were 440C stainless steel discs of 31 mm diameter and 8 mm thickness. Prior to the coating deposition, industrial methodology of grit blasting, cleaning, and then preheating was followed. HVOF (JP-5000 system) spraying was carried out using the parameters industrially optimised for this material (Table 2). The first layer, WC–40%wtNiCrBSiFeC, was deposited onto the substrate to a thickness of 100 µm, and the second WC–10%wtNiCrSiFeBC layer was subsequently applied to achieve a total as-sprayed coating thickness of 500 µm. Coatings were then ground and polished to achieve a total thickness of approximately 400 µm.

### 2.2. Heat-treatment

The heat-treatment was carried out in an argon environment to prevent oxidation of the coating systems. The discs were placed in the furnace, which was evacuated of air, filled with argon and heated at 4 °C min<sup>-1</sup>. The coatings were held for 1 h at 1200 °C before being cooled at a rate of 4 °C min<sup>-1</sup> until 800 °C, and then allowed to cool to room temperature.

Table 1  
Coating and substrate materials

Powder	WC–10%wtNiCrSiBFeC	WC–40%wtNiCrSiBFeC
Particle size distribution, µm	–45+15	–45+20
Apparent density, g/cm <sup>3</sup>	4.42	3.51
WC grain size, µm	3–4	3–4
Powder manufacturing route	Agglomerated and sintered	Agglomerated and sintered
Powder shape	Spherical	Spherical
Alloy composition, %wt	Ni: Bal., Cr: 7.6, Si: 3.6, Fe: 2.4, B: 1.6, C: 0.25	Ni: Bal., Cr: 7.6, Si: 3.6, Fe: 2.4, B: 1.6, C: 0.25
Substrate	440C stainless steel	
Chemical composition, %wt	Fe: Bal., C: 0.86–1.20, Mn: 1.0 max., Si: 1.0 max., P: 0.04 max., S: 0.03 max., Mo: 0.75 max., Cr: 16.0–18.0	

Table 2  
Spraying parameters

Spray gun	JP-5000
Oxygen flow	8931 l/min
Kerosene flow	0.321 l/min
Spraying distance	380 mm
Spraying rate	50 g/min

### 2.3. Powder and coating characterisation

The X-ray diffraction (XRD) analysis through the use of a Siemens D500 diffractometer with Cu Kα (1.5406 Å, step size of 0.02° and dwell time of 2 s) radiations was carried out in order to evaluate the phase composition of the powder, and also to investigate the microstructural modifications brought about by the heat-treatment in both coated layers. The powder and the coatings were also characterised using a scanning electron microscope utilising secondary electron and energy-dispersive X-ray detectors. Microhardness measurements were carried out under a load of 2.94 N using a Vickers microhardness (Mitutoyo-Mvk-H1) test machine.

Elastic modulus and fracture toughness tests were also performed via the indentation method. The indentation modulus was measured using real time displacement of the force indentation curve during a hardness test carried out under a load of 500 mN, and correlated to the Young's modulus using the following equation:

$$E = Y_{\text{HU}}(1 - \nu^2) \quad (1)$$

where  $Y_{\text{HU}}$  is the indentation modulus and  $\nu$  is the Poisson's ratio. Further details of this test method can be found in Buchmann et al. [10]. The load was applied for 20 s and maintained for 5 s. Ten measurements were performed on each coating surface and 30 on each cross-section, which were distributed in 3 lines of 10 measurement points each, at 50 µm, 150 µm and 250 µm, respectively, from the coating's surfaces. A distance of 100 µm between all indentations was ensured to eliminate stress-field effects from nearby indentations.

In order to evaluate the fracture toughness, Vickers indentations were performed on the coating surface. The indentation load was varied from 49.05 to 490.5 N.

Although the length of the cracks did not satisfy the criteria for the calculation of fracture toughness as described by Ostojic et al. [11], qualitative observations using optical microscopy were made on the indentations performed at the highest load.

#### 2.4. Tribological testing

Sliding wear tests were performed in a reciprocating ball on disc configuration. The coatings were ground and polished to obtain an average surface roughness ( $R_a$ ) of  $0.04 \mu\text{m}$ . Before each test, the coating and ball were ultrasonically cleaned in acetone to remove any contaminants and grease, and then dried in air. Dry tests were carried out on a sliding, reciprocating wear machine (Fig. 1) at an ambient temperature of approximately  $21^\circ\text{C}$ . Full details of the test machine can be found in Stoica et al. [12]. The oscillating frequency of the disc was  $1 \text{ Hz}$  ( $60 \text{ rpm}$ ), the stroke  $12 \text{ mm}$ , resulting in an average and maximum velocity of  $24 \text{ mm/s}$  and  $37.7 \text{ mm/s}$ , respectively. The total sliding distance was  $864 \text{ m}$  for the duration ( $10 \text{ h}$ ) of each test. The ball specimens were  $12.7 \text{ mm}$  diameter  $440\text{C}$  steel and  $\text{Si}_3\text{N}_4$  ceramic, properties of which are listed in Table 3. The tests were performed under two loads of  $12$  and  $22 \text{ N}$ . These loading conditions are comparable to the load of e.g.  $25 \text{ N}$  prescribed by ASTM G133-02 for dry tests (procedure A), and also to the load values used for the sliding wear evaluations of WC–cermet coatings in the published literature [13,14].

However, there is always an ambiguity when comparing the test results from various tests or tribological conditions. This ambiguity, especially in the loading conditions, can however be somewhat rationalised by considering the contact stress instead of the actual load. It is worth appreciating that these tests are only employed for the relative ranking of materials and full scale testing is therefore critical in the tribological design process. Nevertheless, some correlation with the loading in engineering components is useful, and the conditions adapted here reflected the contact stress induced in moderately loaded engineering components [15,16]. Corresponding to the beginning of sliding, the mean contact stress was in the

Table 3

The properties of the balls used as counterface in sliding tests

	440C steel	$\text{Si}_3\text{N}_4$ ceramic
Diameter, mm	12.7	12.7
Density, $\text{kg/m}^3$	7769	3165
Weight, g	8	3
Average roughness $R_a$ , $\mu\text{m}$	0.015	0.013
Hardness (HV0.1), $\text{kg/mm}^2$	820	1580

range of  $600$  to  $850 \text{ MPa}$ , depending upon the load and ball material. Preliminary analysis of the wear scar dimensions indicated that after few minutes of testing, once the wear scar forms, these average stress values ranged from  $100$  to  $90 \text{ MPa}$ , which decreased to a lower value of around  $3$  to  $5 \text{ MPa}$  at the end of the test. Hence, for  $99.9\%$  of the test time, the stress state represents the situation of moderately stressed components in the range of  $100$  to  $5 \text{ MPa}$ , e.g. gate valves have been shown to be subjected to a contact stress range of  $50$  to  $200 \text{ MPa}$  [15]. Similarly, medical hip implants can be subjected to a contact stress range up to  $55 \text{ MPa}$  [16], which is significantly lower than the high contact stress of few  $\text{GPa}$  seen in rolling/sliding contacts.

The frictional force was also recorded during each test and the friction coefficients were correspondingly computed. The volume loss of each coating wear scar in  $\text{mm}^3$  was measured using Zygo NewView 5000 interferometer. The corresponding ball volume loss was calculated using the following geometrical relations:

$$V = \frac{\pi H^2}{3} (3R - H), \quad (2)$$

where  $H = R - \sqrt{R^2 - r^2}$  and  $R$ ,  $r$  are the ball radius and ball-wear-scar radius, respectively. With the help of optical microscopy precise measurement of the ball-wear-scar radius was possible. This methodology is consistent with the ball volume loss calculations adapted in ASTM G99 and ASTM G133-02. The wear scars and debris were examined by optical and scanning electron microscopy. Each test was repeated at least three times to verify the reproducibility of wear results.

### 3. Experimental results

#### 3.1. Microstructural identification

##### 3.1.1. X-ray diffraction analysis

Fig. 2 shows the XRD spectra of the spray powder, as-sprayed, and heat-treated coatings. The spectra of the two powder compositions are displayed in Fig. 2a. The main peaks are tungsten carbide (WC) for both compositions. As expected, higher intensities of these peaks were recorded for WC– $10 \text{ wt.}\%$  Ni alloy powder. Beside the carbide phase, the spectra revealed amounts of metallic nickel and/or chromium. Additionally some amounts of chromium carbide ( $\text{Cr}_7\text{C}_3$ ) were detected by X-ray diffraction, i.e. a phase

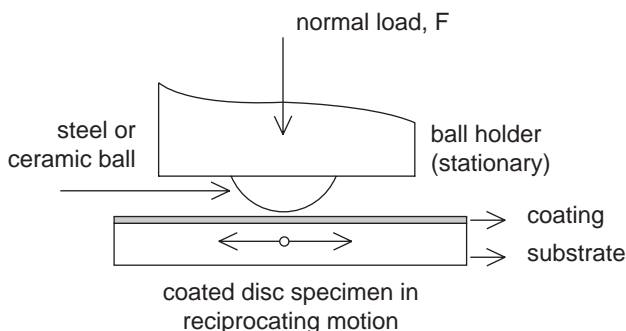


Fig. 1. High frequency reciprocating ball on plate rig.



40°. As expected the top layer shows significantly higher amount of the decomposition products. There are a couple of peaks which indicate the state of the matrix after deposition. The peak located at about 43.5° ( $2\theta$ ) corresponds to the  $\text{Cr}_3\text{Ni}_2$  and/or  $\text{NiC}_x$  and was observed on both coating layers. The peak at approximately 44° ( $2\theta$ ) on the bottom layer was identified as chromium carbide ( $\text{Cr}_{23}\text{C}_6$ ).

The spectra of the heat-treated coating shows a number of complex tungsten carbide phases, which formed on both coating layers. These phases ( $\text{Ni}_2\text{W}_4\text{C}$ ,  $\text{FeW}_3\text{C}$ ,  $\text{Fe}_6\text{W}_6\text{C}$ ) have been produced on the expense of primary tungsten carbide (WC), secondary tungsten carbide ( $\text{W}_2\text{C}$ ), and metallic tungsten (W). In addition to these phases, the spectra reveals reactions within the matrix, which resulted in new phases such as nickel boride ( $\text{Ni}_4\text{B}_3$ ), chromium borides ( $\text{CrB}_6$ ,  $\text{Cr}_2\text{B}_3$ ), and chromium carbides ( $\text{Cr}_3\text{C}_2$ ,  $\text{Cr}_7\text{C}_3$ ).

### 3.1.2. SEM observations

Scanning electron micrographs of the as-sprayed coatings are presented in Fig. 3. Fig. 4 shows the micrographs of the heat-treated coating. These figures show the main features of the two coatings, highlighting the difference between them at higher magnification. Figs. 3a and 4a provide an overall view of the coating substrate systems. The micrograph of the as-sprayed coating clearly reveals the boundary between the top and the bottom coating layers, and the interface separating the coating and the substrate. Contrary to this, the micrograph of the heat-treated coating, intentionally taken at slightly higher magnification for illustrative purposes, shows couple of additional interfacial layers, first of about 50  $\mu\text{m}$ , which formed between the coating layers (Fig. 4a) and the second one, whose thickness is about 20  $\mu\text{m}$ , which formed between the bottom layer and the substrate (Fig. 4c).

Closer examination under SEM indicated significant changes experienced by the coating constituents after being heat-treated at 1200 °C. Figs. 3b and 4b show the dissimilarities between the structures of the as-sprayed and heat-treated coatings, particularly in the bottom layer. The WC grains have well defined corners and edges (prismatic features) as opposed to the morphology observed on the as-sprayed coatings. Moreover, as illustrated in the left insert of Fig. 4b, characteristic of the bottom layer of the heat-treated coating were darker areas located in the close vicinity of the carbide grains, as seen in the backscattered image.

### 3.2. Mechanical testing

#### 3.2.1. Microhardness measurements

The results of the microhardness measurements are presented in Fig. 5. Hardness values quoted are an average of 30 measurements which were performed on the coating surface, and on five lines distributed along the cross-section at 50  $\mu\text{m}$  from the interface on the substrate, and at 50  $\mu\text{m}$ , 150  $\mu\text{m}$ , 250  $\mu\text{m}$  and 350  $\mu\text{m}$ , respectively, from the interface on the coating cross-section. Fig. 5 shows the

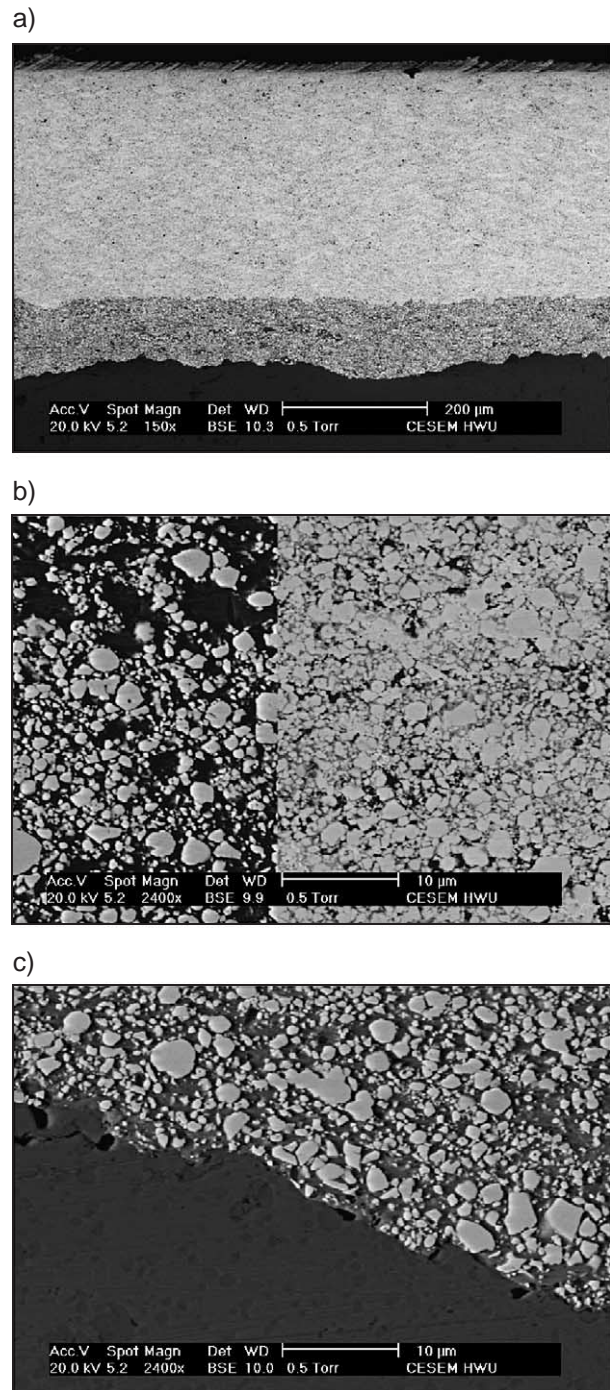


Fig. 3. SEM micrographs of the as-sprayed coating: a) general overview, b) coating cross-section: left insert—bottom layer, right insert—top layer and c) interface between the coating and the substrate.

variation in the microhardness with the coating heat-treatment and, for each coating, the variation of the microhardness through the thickness. The results of the measurements performed on the substrate, in the close vicinity of the interface with the bottom layer, show higher microhardness of the steel substrate after the heat-treatment.

Interestingly, the bottom layer of the heat-treated coating exhibits lower microhardness than that of the as-sprayed

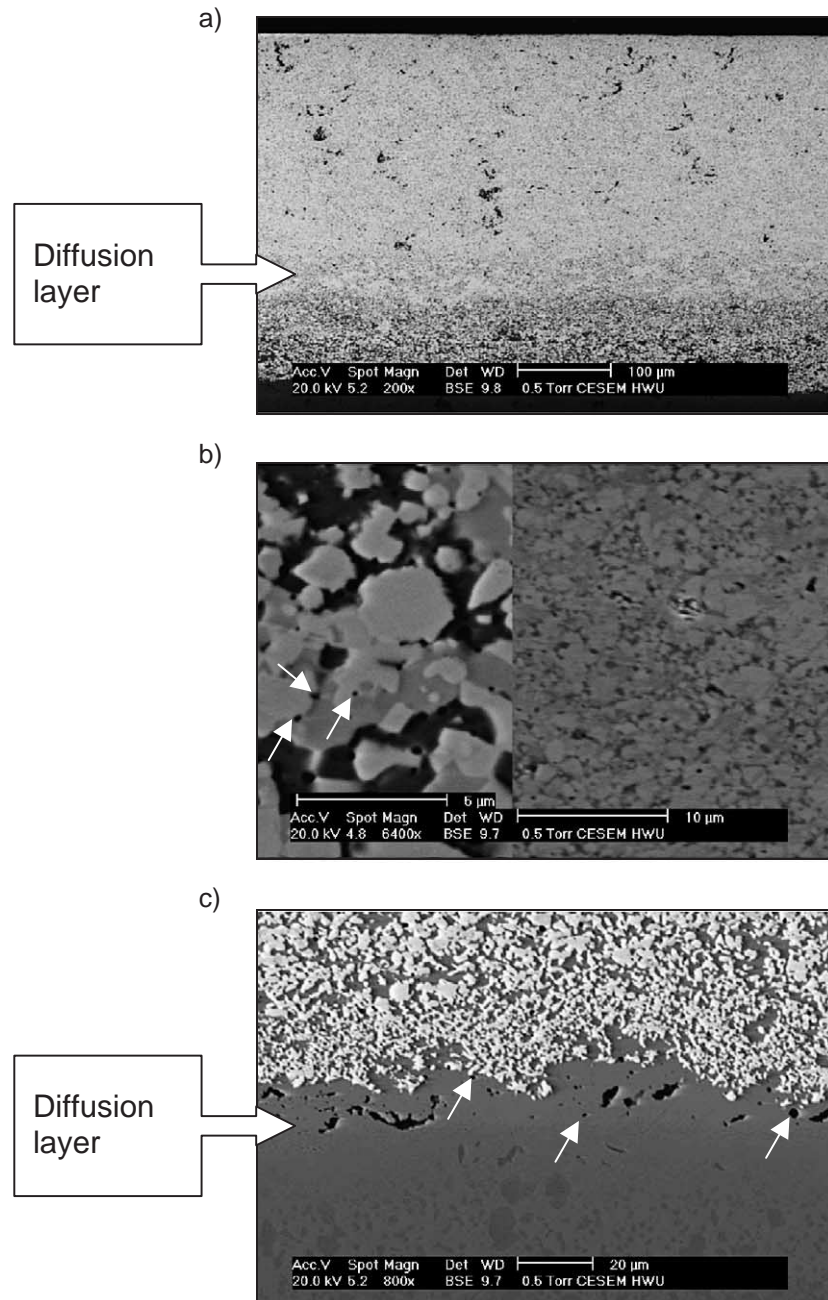


Fig. 4. SEM micrographs of the heat-treated coating: a) general overview, b) coating cross-section: left insert—bottom layer, right insert—top layer and c) interface between the coating and the substrate (arrows mark the location of some Kirkendall pores).

coating. Thus, after the heat-treatment, there is a drop in the microhardness of the coated bottom layer from an average of 1130 HV<sub>300</sub> to approximately 900 HV<sub>300</sub>. However, the expected increase in the microhardness with the heat-treatment occurred in the top coated layer, where the average value of the microhardness on the entire thickness was found to be around 1450 HV<sub>300</sub>, with an ascending trend towards the coating surface. However considering the scatter in the results, it can be appreciated that regardless of the coating type, there is not much variation in microhardness with coating thickness.

The measurements performed on the surface of the two coatings indicated less difference in the microhardness between the as-sprayed and heat-treated coatings. Although there was an increase of about 20% in the average value determined for the heat-treated coatings, the overlapping error bars indicate less difference between the two coatings.

### 3.2.2. Fracture toughness measurements

The evaluation of coating fracture toughness was carried out by qualitative observations of the indentations performed at 490.5 N. Fig. 6 illustrates the main differences in

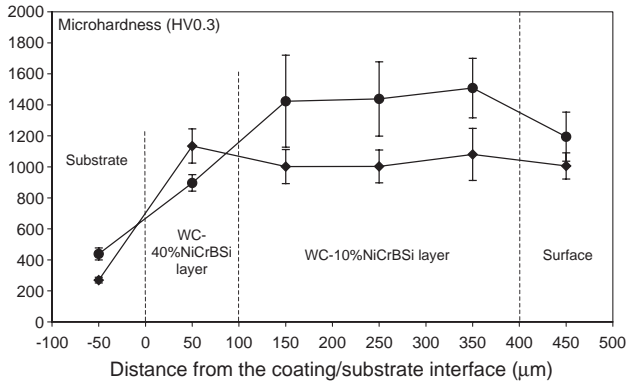


Fig. 5. Variation of coating microhardness with the distance from the coating/substrate interface. ♦ as-sprayed, ● heat-treated coatings.

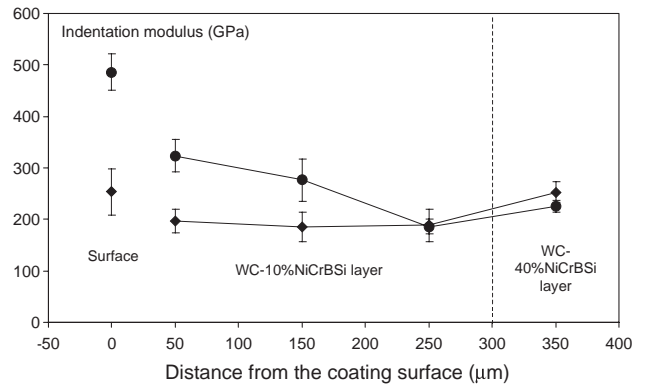


Fig. 7. Variation of indentation modulus with the distance from the coating surface. ♦ as-sprayed, ● heat-treated coatings.

the size of the indentations, and the crack behaviour observed especially in the case of as-sprayed coatings. As indicated in Fig. 6a, the indentation performed on the as-sprayed coating is surrounded by cracks that originated either from the corners or along the sides of the indentation, propagating randomly around indentation. Contrary to this, the indentation performed on the heat-treated coating did not show any visible cracks.

It is worth appreciating that at the highest load of 490.5 N used for this investigation, the size of indentation diagonal was approximately 300 µm. Even at this load no cracks were observed in the post-treated coating. As the thickness of the top WC–NiCrBSi layer was approximately 300 µm, through thickness quantitative analysis of fracture toughness, as reported by Ostojic et al. [11], Lima et al. [17] and Lopez et al. [18] could not be applied. However, even if such analysis was possible, the high value of scatter reported in these previous investigations [17,18] have shown that the exact value of fracture toughness can significantly vary due to the complexity in the coating microstructure.

### 3.2.3. Indentation modulus measurements

Fig. 7 shows the results of indentation modulus measured through-depth, and on the surface of both the as-sprayed and heat-treated coatings. Throughout the cross-section of the as-sprayed coating’s top layer, modulus maintains a rather

constant value of around 200 GPa. Relatively higher value with an average of about 250 GPa was obtained for the bottom layer. Measured on the coating surface, the modulus was about 250 GPa with slightly higher scatter than in the through thickness measurements.

The measurements carried out on the heat-treated coating gave a peculiar trend. The bottom layer of the heat-treated coating had a relatively lower indentation modulus, as opposed to the bottom layer of the as-sprayed coating. However, for the rest of the measurements, significantly higher modulus was found. The highest increase was measured on the coating’s surface where a high average value of about 480 GPa was achieved.

### 3.3. Tribological testing

#### 3.3.1. Friction behaviour

Traces of friction coefficients for each of the tested couples are shown in Fig. 8. Typical friction behaviour was recorded in all cases, i.e. running-in stage, the duration of which varied depending on the couple and load used, and the stabilisation stage, characterised by a rather stable friction coefficient. Although fluctuations were recorded for most of the tested pairs, they were quite significant in the couples involving ceramic balls, and were indicative, amongst other factors, of the role of wear debris within the contact region.

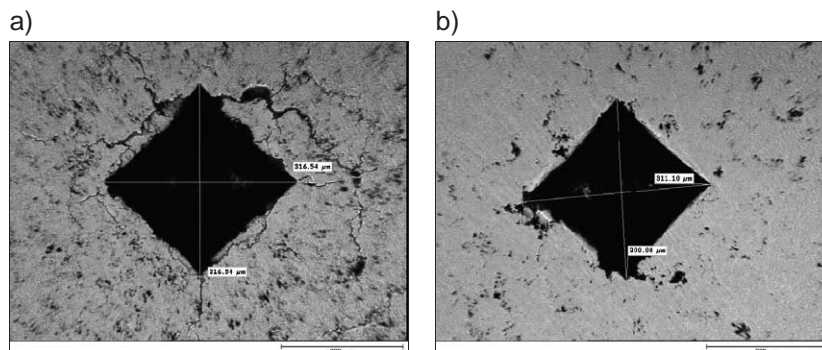


Fig. 6. Fracture toughness indentations on a) as-sprayed and b) heat-treated coatings.

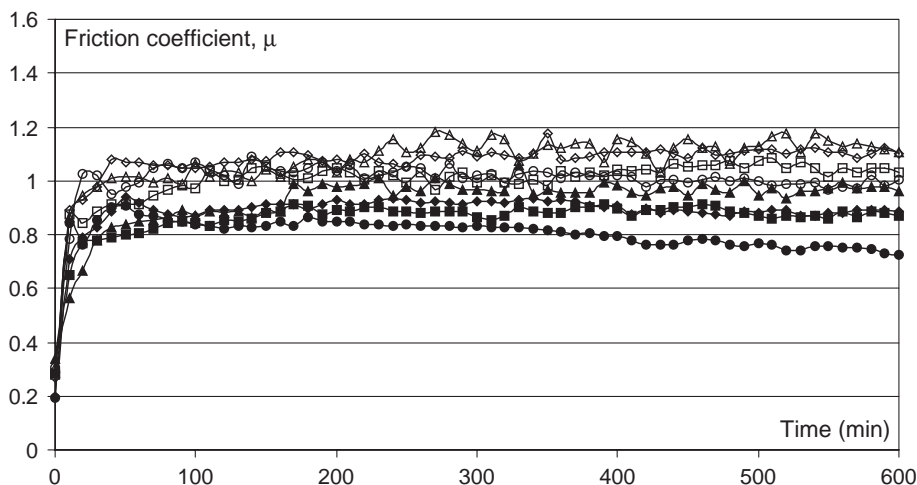


Fig. 8. Friction coefficient of the as-sprayed tested against steel ( $\diamond$ —12 N,  $\blacklozenge$ —22 N), ceramic ( $\triangle$ —12 N,  $\blacktriangle$ —22 N) and heat-treated tested against steel ( $\circ$ —12 N,  $\bullet$ —22 N), ceramic ( $\square$ —12 N,  $\blacksquare$ —22 N).

The influence of the applied load on the friction coefficient can also be appreciated from Fig. 8. Regardless of the test couple, the resulting friction was higher when low load was used. Thus, steel/as-sprayed couple gave an average friction coefficient of about 1.1 and 0.85, when they slid under 12 and 22 N, respectively. Similarly, ceramic ball against the as-sprayed coating under low load gave a friction coefficient of about 1.12, while only 0.96 was recorded during the higher load test. Heat-treated coatings tested against steel balls produced friction coefficients of 1.01 and 0.8, whilst when tested against the ceramic ball, 1.03 and 0.88 was recorded for the low and high load tests, respectively. These values were determined by averaging the friction coefficients over the stabilisation stage of each test. Hence these values indicate a rather consistent but unexpected behaviour, i.e. friction decreases with the increase in the applied load.

Following the values of friction coefficients provided above, there was no significant difference in the friction when different counter bodies were used. Although the average of friction coefficient is slightly higher in the tests involving ceramic balls, the difference was rather insignificant. Fig. 8 however shows the dependence of friction on the coating heat-treatment. The couples involving as-sprayed coatings produced noticeable higher friction coefficients. This behaviour was consistent regardless of the test parameters (load, counterbody).

### 3.3.2. Sliding wear

The volume loss of the coating material, as provided by the interferometric measurements, appears to be correlated with the friction coefficients. Fig. 9 shows the relative wear performance of the heat-treated and as-sprayed coatings. Under the tribological conditions employed in this study, the as-sprayed coatings lost relatively higher material as opposed to the post-treated coatings.

Sliding wear test results indicated that, regardless of the applied load, the ceramic counterbody removed less material from the heat-treated coatings, compared to the steel ball. Considering the variation of the results, when as-sprayed coatings were used, there was no significant difference. As for the effect of the applied load on the coating volume loss, the increase of load from 12 to 22 N almost doubled the amount of material loss.

Apart from the coating volume loss, the total volume loss of the contacting pairs was also computed, by adding the material loss of the corresponding balls. These results of the ball material loss and total volume loss are displayed in Fig. 10a and b, respectively, for both the steel and ceramic balls. Interestingly, beside higher coating volume loss, the couples involving the as-sprayed coatings also produced higher volume loss of the balls. This behaviour was seen for all test couples regardless of the type of the ball or load used. Thus, when steel/as-sprayed couple slid under 12 and 22 N, the volume of steel removed from the ball was 0.55 mm<sup>3</sup> and 0.91 mm<sup>3</sup>, respectively. Comparing, only 0.061 mm<sup>3</sup> and 0.17 mm<sup>3</sup> were measured when steel/heat-treated coating couple was tested. As seen in Fig. 10a, volume of ball material removed was an order of

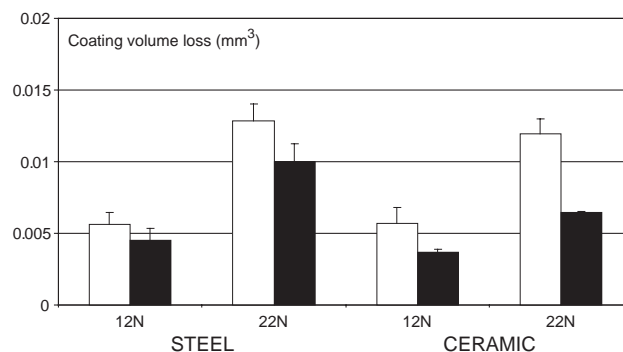


Fig. 9. Coating volume loss (mm<sup>3</sup>).  $\square$  as-sprayed,  $\blacksquare$  heat-treated coatings.

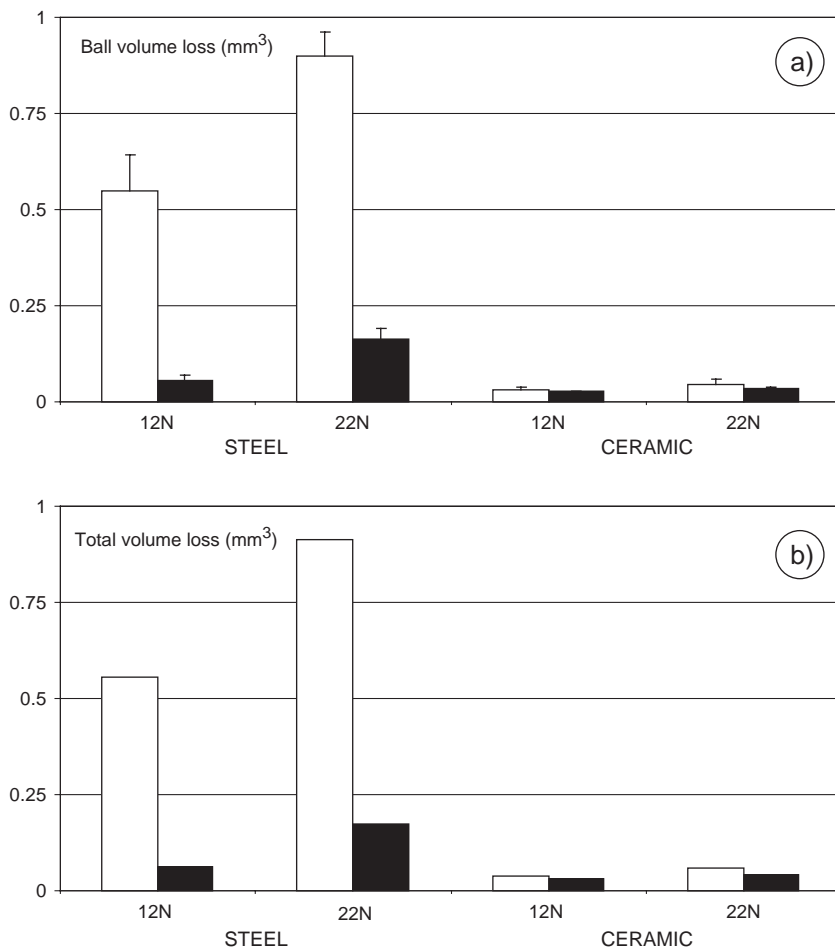


Fig. 10. a) Ball volume loss ( $\text{mm}^3$ ) and b) Total volume loss ( $\text{mm}^3$ ). □ as-sprayed, ■ heat-treated coatings.

magnitude less when ceramic balls were used. Also less difference was recorded between the volume loss produced using the as-sprayed and heat-treated coatings at both 12 and 22 N.

Fig. 11 shows the SEM observations of the wear tracks of the as-sprayed and heat-treated coatings for various test couples. The EDX analysis of the dark regions seen on the wear tracks is shown in Fig. 12 for the coating–ceramic couples. The morphology of the wear debris collected at the end of the wear tests is shown in Fig. 13.

#### 4. Discussion

The wear performance of thermally sprayed coatings, in particular tungsten carbide coatings, is related to the extent of the phase transformations within the microstructure during the process of powder deposition. When the desired coating properties are still to be achieved, post-treatments can be employed to promote further microstructural changes and alter wear properties. In the following, the effect of sintering and diffusion caused by the heat-treatment on the coating microstructure, mechanical properties, and sliding wear performance is discussed.

##### 4.1. Coating microstructure

The XRD analysis (Fig. 2) performed on the powders for both layers indicated that both powders had WC as the main constituent, with higher amounts of Ni, Cr and Cr-carbide in the bottom layer, which was due to the differences in composition of the two powders. The deposition of the powder using JP-5000 system under the conditions summarised earlier (Table 2) generated a number of transformations in the coating microstructure. The combined effect of several mechanisms was responsible for the new phase configuration. At the flame temperature of spraying, Ni alloy melts promoting tungsten carbide (WC) phase dissolution. At the same time, oxidation-driven decarburisation of WC takes place at the surface of particles to the extent that both  $\text{W}_2\text{C}$  and W form. The exact mechanism of oxidation driven reactions can be appreciated from Lovelock [19] and Verdon et al. [20]. These mechanisms indicate either direct carbon interaction with oxygen during spraying or through dissolution of WC grains followed by diffusion of carbon towards the surface of particles, and carbon oxidation. Verdon et al. [20] also suggested that as the particle temperature increases, the WC solubility in liquid also increases, resulting in a nano-crystalline (W–Co–C)

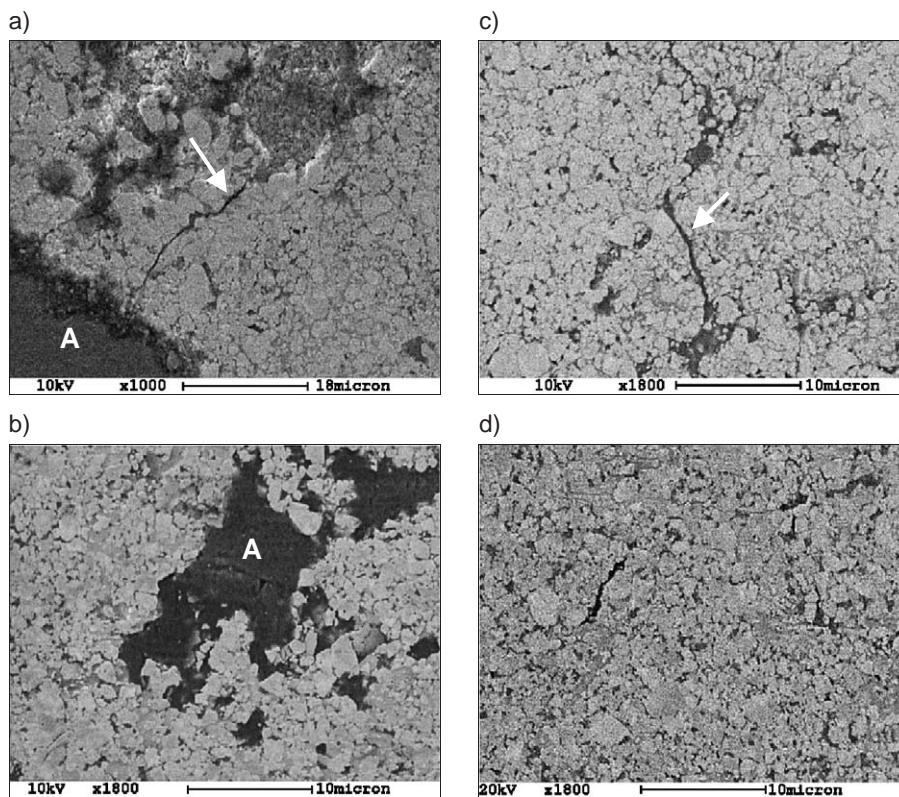


Fig. 11. SEM micrographs within the wear scar of as-sprayed and heat-treated coatings tested against steel—a, b) and ceramic c, d) under a load of 22 N (“A” indicates oxide layers, arrows indicate cracks).

binder phase during rapid cooling. However, as no peak broadening was appreciated in the as-sprayed WC–NiCrBSi coatings (Fig. 2b), it is not clear if such mechanisms of nano-crystalline binder phase were dominant during the spraying of the WC–NiCrBSi coatings. Moreover, as the matrix composition is complex, it is not clear if the thermal kinetics favoured the solubility of WC to form nano-crystalline phase between W–Ni–C–Cr. The temperature reached during spraying process however promoted reactions within the matrix, such as the reaction between chromium and nickel ( $\text{Cr}_3\text{Ni}_2$ ) and also between chromium and carbon ( $\text{Cr}_{23}\text{C}_6$ ).

The XRD analysis performed on the bottom layer revealed a reduction in the intensities of most of the WC phases seen in the top layer. Less amount of primary carbide in the powder, that formed the bottom layer, was reflected throughout the spectra in peaks having less WC intensity. Consequently it led to a decrease in the reactions involving WC phase. This was confirmed by the absence of some  $\text{W}_2\text{C}$  peaks in the spectra of the bottom layer, and reduction in the intensity of those that were present.

XRD investigations also showed that the sintering and diffusion during the heat-treatment carried out at 1200 °C produced changes in the phase composition of both coated layers. In the top layer, a reduction in the intensity of primary tungsten carbide (WC) was identified along with the elimination of  $\text{W}_2\text{C}$  and W peaks. The high temperature

during the heat-treatment promoted a series of reactions that resulted in the occurrence of a number of new phases. They were indexed as complex carbides ( $\text{Ni}_2\text{W}_4\text{C}$ ,  $\text{FeW}_3\text{C}$ ,  $\text{Fe}_6\text{W}_6\text{C}$ ), products of reactions between the WC,  $\text{W}_2\text{C}$ , W, and also Ni and Fe from the matrix. Moreover, the XRD spectra of the heat-treated sample showed indications of reactions within the matrix. New peaks were recorded and were identified as boron nickel, chromium boron and chromium carbide phases. These phase transformations altered the mechanical properties of the coating. Although it was seen that there was a decrease in the relative intensity of WC peaks after the heat-treatment, it can be appreciated that the formation of complex tungsten carbides, balanced the loss of hardness, expected as a result of the loss of some of the primary tungsten carbide (WC). Hence, the hardening of the matrix around the carbide grains brought extra hardness to the coating. Previous investigations (e.g. [2–4]) have shown that the new nickel and chromium phases, which form in the matrix, increase the hardness of the material whose constituents they are. It is therefore expected that these transformations would cause an increase in the coating hardness, as observed in Fig. 5.

The behaviour was however different in the lower layer. This was due to the lower WC content, and the formation of diffusion layers at two locations, i.e. between the two (top and bottom) coating layers, and also at the coating substrate interface. After the heat-treatment, there was a further

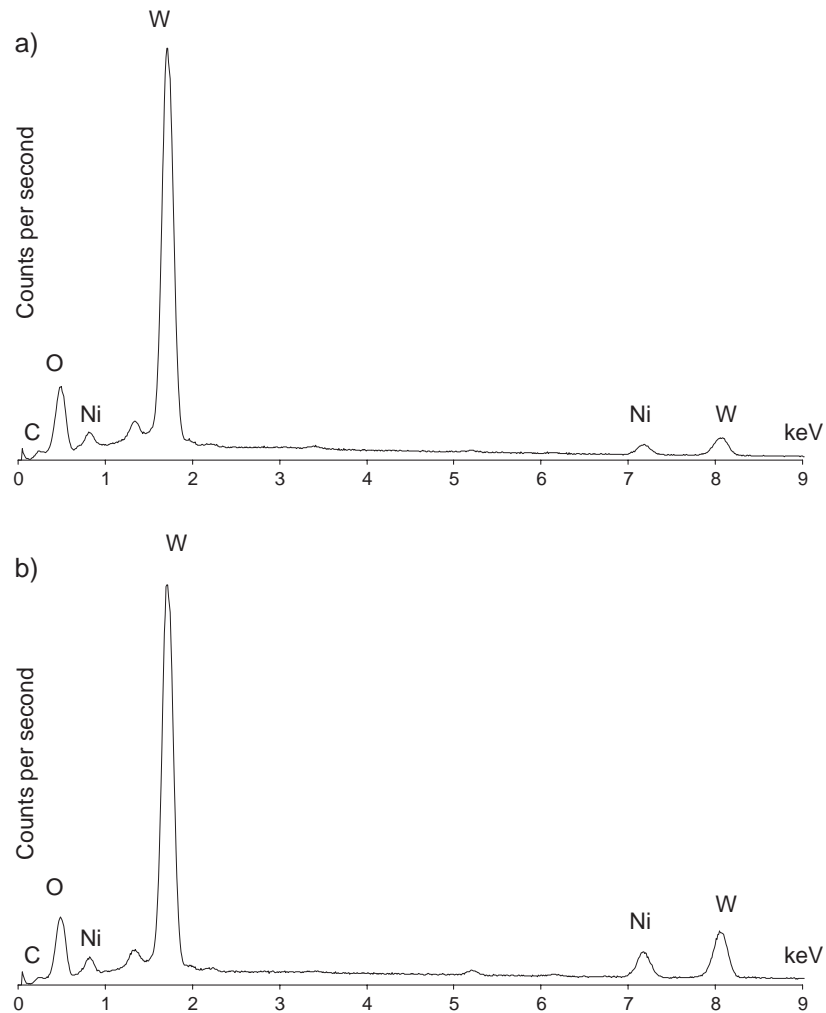


Fig. 12. EDX analysis within the wear scar of a) as-sprayed and b) heat-treated coatings tested against ceramic ball (load—22 N).

decrease in the relative intensity of WC peaks, suggesting, as mentioned before, transformations that involved primary carbide and matrix. However, the formation of diffusion zones altered the rate of reactions resulting in an overall decrease in the average microhardness of the lower layer.

Figs. 3 and 4 illustrate the microstructure of the as-sprayed and heat-treated coatings, highlighting the changes brought about by heating the coated sample at 1200 °C. As shown in Fig. 3, there is a clear interface between the substrate and the bottom coating layer of the as-sprayed coating. Contrary to this, the boundary was eliminated in the heat-treated coating due to the formation of an interfacial layer of about 20  $\mu\text{m}$  thickness. The existence of this additional layer was further confirmed by the elemental analysis (EDX) carried out on the substrate, neighbouring the initial interface. Although not reported here, preliminary analysis of these coatings indicated that the thickness of this diffusion zone increased with the heat-treatment time. Within this diffusion zone, it was found that considerable amount of Ni was present, suggesting that diffusion-controlled processes took place, leading to a metallurgical bonding between the bottom layer and the substrate. Hence,

it was expected that there will be improvement in the coating's adhesive strength, and microhardness of the steel in the close vicinity of the bottom layer. This expected increase in substrate hardness near the coating substrate interface was further confirmed by the microhardness measurements shown in Fig. 5.

Similarly, there was another diffusion layer which formed between the top and bottom coating layer. Again the thickness of this diffusion zone was a function of time, which was confirmed by the preliminary analysis. There was another feature which was noticed throughout the diffusion layer. This was the presence of a number of pores also called the Kirkendall pores [21]. This is based on unequal diffusion between the bottom coated layer and substrate, causing an excess of vacancies, which ultimately become pores (Kirkendall pores), as shown in Fig. 4.

#### 4.2. Mechanical properties

The changes in coating's mechanical properties were closely related to the transformations in the coating microstructure during the heat-treatment. As mentioned in the

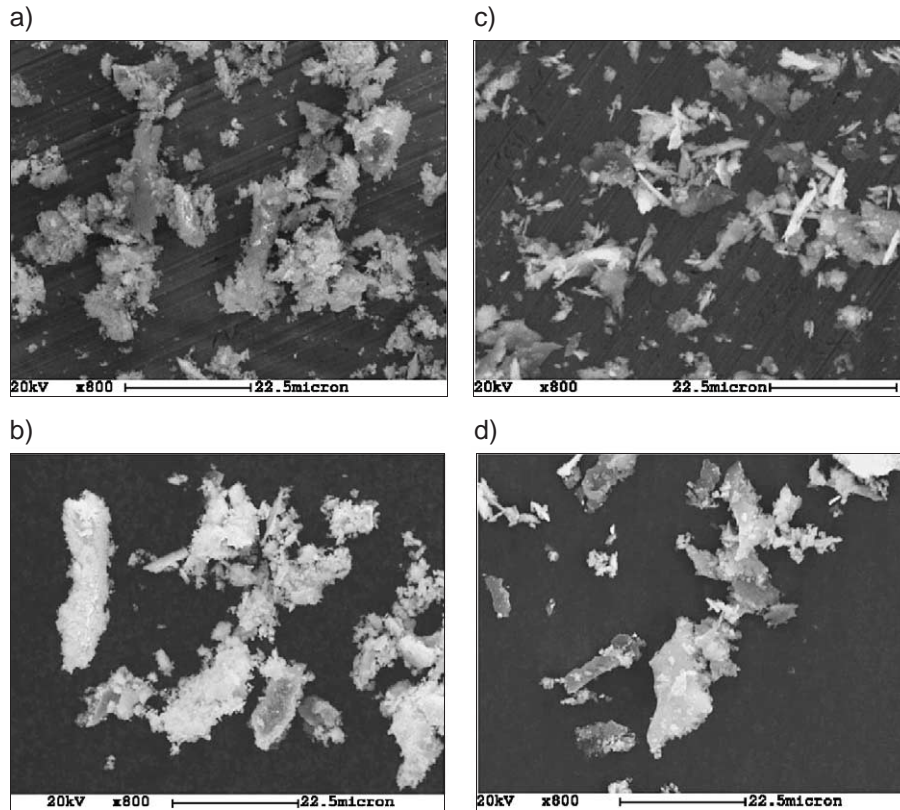


Fig. 13. Debris formed by sliding the as-sprayed and heat-treated coatings against steel—a), b), c) and ceramic balls d), e), f). Load—12 N.

previous section, the increase in the hardness of the top coated layer was attributed to the matrix hardening following the heat-treatment. Qualitative analysis of fracture toughness measurements shown in Fig. 6 also indicated improvements in coating's fracture toughness after the heat-treatment. The elimination of brittle secondary tungsten carbide ( $W_2C$ ) and metallic tungsten (W), metallurgical intersplat bonding, and possible role of residual stress are some of the factors influential for such improvements. Nevertheless, one should expect toughness to increase inversely with hardness, however, the change in coating's elasticity (Fig. 7) was responsible for the simultaneous increase of both the hardness and toughness. Although slightly higher than expected on the coating's surface, the results of indentation modulus on the top layer confirmed that the heat-treatment resulted in an improved bonding within the coating microstructure.

As-sprayed coatings showed an average modulus in the range of 200–240 GPa, which is consistent with the modulus measurements of thermally sprayed WC–cermet coatings reported by Tucker [22], Brandt [23], and also follow the general rule reported by Kuroda et al. [24], which indicated that the modulus of sprayed deposit is generally one-third of the bulk material. After the heat-treatment, on the surface and on the regions of the top layer neighbouring the coating surface, the results show dramatic increase in the coating's elasticity. On the coating surface, the indentation modulus of 486 GPa gives a Young's modulus of about 466

GPa, assuming a Poisson's ratio of 0.2 (Eq. (1)), which is significantly higher than the usual value of thermal sprayed WC-based cermet coatings (200–240 GPa). However this value is still lower than the bulk WC–Co cermet modulus of around 580 GPa [25]. Although the anisotropy inherent to as-sprayed coatings shown in Fig. 7 increased after the heat-treatment, as indicated by the large variations in coating's elasticity, it is believed that once the coating underwent transformations in the phase composition, the bonding mechanism improved and metallurgical bonds formed due to sintering via diffusion, causing an increase in the coating elasticity. Other mechanisms of sintering, i.e. alloying, densification, grain growth and liquid phase sintering, are also expected to contribute at this sintering temperature, details of which are not discussed here. It is however believed that this variation in modulus through thickness is not only governed by the different rates of reactions during sintering, but also the role of residual stress following the heat-treatment, as previously reported for post-treated WC–cermet coatings [26,27].

#### 4.3. Tribological testing

The effect of heat-treatment on the wear behaviour of WC–NiCrBSiFeC coating was examined in sliding conditions. As mentioned earlier in Section 3.3, the heat-treated coatings lost less volume of material than the as-sprayed ones, regardless of the load or counterbody (Figs. 9 and 10).

The results of the friction measurements (Fig. 8) indicated similar behaviour, i.e. independent of the tribological conditions, the friction coefficients recorded on the heat-treated coatings were lower than those of the as-sprayed ones. The rationale of these differences in the wear and friction performance after the heat-treatment is explained in the following due to the simultaneous improvement in coating's hardness, toughness, and modulus, and by relating it to the wear mechanisms that operated in each test couple.

The difference in the friction and volume loss between the as-sprayed and heat-treated coatings, regardless of the tribological conditions, was given by the extent, and also the synergetic effect of individual wear mechanisms, e.g. oxidation, two-body and three-body abrasion, carbide pull-out, and fracture. Given the improvement in coating's hardness after the heat-treatment, it was not surprising to see an improvement in coating's wear resistance due to the influence of hardness on both the two- and three-body abrasion [28], especially where plasticity is involved as a wear mechanism. However, hardness alone was not responsible for the improvements seen in coating's wear performance. There was an additional wear mechanism operational only when the as-sprayed coatings were tested, which increased the material loss not only for the as-sprayed coatings, but also for the coupled balls. This was microcracking and was caused by the relatively brittle microstructure of the as-sprayed coating. This difference was attributed to a relatively lower fracture toughness of the as-sprayed coatings (Fig. 6). Thus under the contact load, the cracks initiated within the wear track, propagating along the boundaries of WC grains (Fig. 11a), preferentially perpendicular to the sliding direction. This preferential direction of cracking indicated that the cracks were likely to be initiated by the tensile stress at the edge of the contact zone. This also indicated that the as-sprayed coatings were much weaker in tension than in shear. However, given the coefficient of friction of 0.8 to 1.0, seen for the various test couples, the maximum shear stress can also migrate to the surface due to traction, and hence initiate crack propagation. These cracks were quite detrimental for the integrity of both the coating and the coupled ball, and hence significantly influenced the wear and friction mechanisms of the as-sprayed coatings. Beside the fact that the coating neighbouring the cracks was prone to further wear, the crack's sharp edges produce extensive damage to the coupled ball. The extent of this damage was also dependent on the hardness of the ball. Moreover, under subsequent sliding, the microcracks formed nets, which ultimately led to coating spallation/delamination. In terms of friction, microcracking as an energy dispersive mechanism increased the friction of the system in the as-sprayed coatings, as shown in Fig. 8.

It was also noted that the friction coefficient decreased with the increase in the applied load. This was inconsistent with Coulomb's friction [28], which states that friction coefficient does not depend on the test load. However, the

independence of friction upon the applied load was not seen for the particular coupled materials, and test conditions, used in this investigation. It is believed that two factors were responsible for this behaviour, i.e. role of debris within the contact region, and the influence of oxide film.

Microanalysing the worn coating surfaces under scanning electron microscope it was found that dark layers, labelled 'A' in Fig. 11, were randomly distributed within the wear scars. Elemental analysis (EDX) performed on these dark layers indicated large amounts of oxygen, suggesting the presence of oxides (Fig. 12—coating against ceramic balls). They are believed to be tungsten oxides ( $WO_3$ ) when ceramic balls slid on the coatings, and iron oxide (FeO) when coatings slid against steel balls, although in this case tungsten might also have been oxidized. There is also a possibility that FeO formed when coating slid against ceramic balls. This was due to the presence of Fe in the coating matrix (Table 1). However, since no Fe peaks were seen in the EDX analysis shown in Fig. 12 for the coating ceramic couple, the extent of FeO formation might have been very limited for this test couple. Thus, regardless of the type of the coating, during sliding, high flash temperatures were reached which promoted the oxidation at asperity level. It is however not clear if the extent of oxidation was influenced by the heat-treatment. Nevertheless, the oxide layers lowered the severity of the contact by acting as solid lubricant. Therefore once oxidation took place, a decrease in the friction and wear of the coupled pair occurred. This was also partly responsible, apart from the role of debris within the contact region, for the fluctuations seen in friction for various test couples during the tests (Fig. 8). However, the beneficial role of the oxide layers depended on their ability to withstand the load applied by the ball during further sliding, and once removed, by the rapidity of the formation of the new layer.

SEM micrographs of these dark layers indicated smearing, suggesting that after their formation, these layers were spread over the coating wear track. Some of this oxide layer filled into the surface pits, providing the system with additional solid lubricant, while the remaining transformed in thinner layers. Under the applied load, the coating however ultimately spalled off and fragments were removed from the contact area. Some of these fragments adhered to the previously formed debris, further altering the wear and friction of the system in three-body abrasion.

The typical appearance of a material that underwent abrasive wear was seen on all tested coatings and steel balls. Parallel grooves running in the sliding direction were seen under the optical microscope, which indicated that plastic deformation occurred, regardless if as-sprayed or heat-treated coatings were involved in the test couple. However, it is believed that the improved mechanical properties of the heat-treated coatings, inhibited the process of plastic deformation (microcutting) as part of abrasive wear, ensuring therefore less material loss for the heat-treated system.

Fig. 13 shows the typical debris found after testing under different conditions. Some particles were removed from the contact area after their formation, while some were trapped within the contact area for certain amount of time, resulting in different shapes and sizes. Some are agglomerations of fine particles while others are flake-like particles of different sizes. Elemental analysis performed on these particles indicated amounts of oxygen, suggesting they contain fragments of oxides. The flake-like particles were seen for all tested couples and the agglomerations of fine particles were particularly seen in the tests that involved steel balls. As discussed before, during sliding, detachment of coating/ball particles occurred. Flake-like debris were thus produced which were fragmented as the wearing process progressed. Elemental analysis taken on these particles showed approximately the same composition as on the agglomerations of fine particles. They contained, beside the oxide, fragments of coating and ball material.

Hence, each wear mechanism had its own contribution to the friction and wear of the system. The combination of these contributions resulted in the friction and wear behaviour shown in Figs. 8–10. Microcracking, abrasive wear, and matrix carbide pull-out (fracture) were the energy dispersive wear mechanisms, and therefore contributed to the differences in the friction of various test couples. The differences seen in the friction and also the wear of the as-sprayed and heat-treated coatings was thus a reflection of the extent of these wear processes. The difference in the degree of damage caused by any of the above-mentioned processes was due to the alteration of the coating microstructure during the heat-treatment, i.e. the hardening of the binder and the improvement of the bonding between the carbides, and the matrix inhibited the abrasive and carbide pull-out (fracture) mechanism, whereas the elimination of brittle phases led to the absence of microcracking as a source of damage mechanism.

## 5. Conclusions

The microstructure, mechanical properties, and sliding wear of the as-sprayed and heat-treated thermally sprayed WC–NiCrBSiFeC coatings were evaluated in order to investigate the potential of heat-treatment to improve coating's wear resistance. This investigation shows that under different tribological conditions, not only the volume loss of the coatings, but also the total volume loss of the test couples decreased after the heat-treatment. This increase in the wear resistance was attributed to the simultaneous increase in coating's hardness, toughness, and elasticity as a result of the following changes which occurred within the coating microstructure:

1. The formation of complex carbides by dissolution of primary carbide (WC) in the matrix, and the occurrence of other hard phases as a results of reactions within the

matrix, which increased the hardness of the heat-treated coatings.

2. The elimination of the brittle phases ( $W_2C$  and W) which were seen in the as-sprayed coatings, which was partly responsible for the improvement in coating's fracture toughness.
3. Once phase transformations occurred in the coating, metallurgical bonds developed both at the intersplat and also at the coating substrate interface levels, as observed by the improvement in elastic modulus and formation of diffusion zones.
4. Considerable diffusion was seen to occur at the interface between the lower coated layer and the steel substrate indicating a metallurgical bonding.

## Acknowledgements

Authors would like to thankfully acknowledge the financial support of EPSRC (Grant Number GR/R45284) in this project.

## References

- [1] I.C. Grigorescu, C. Di Rauso, R. Drira-Halouani, B. Lavelle, R. Di Giampaolo, J. Lira, *Surf. Coat. Technol.* 76–77 (1995) 494.
- [2] Z. Ding, H. Zhao, J. Wang, in: C.C. Berndt, K.A. Khor, E.F. Lugscheider (Eds.), *Thermal Spray 2001: New Surface for a New Millennium*, ASM International, ISBN: 0871707373, 2001, p. 1089.
- [3] M. Rodriguez, J. Klisans, L. Bavaresco, A. Scagni, F. Arenas, in: C.C. Berndt, K.A. Khor, E.F. Lugscheider (Eds.), *Thermal Spray 2001: New Surface for a New Millennium*, ASM International, ISBN: 0871707373, 2001, p. 1061.
- [4] S.C. Modi, E. Calla, in: C.C. Berndt, K.A. Khor, E.F. Lugscheider (Eds.), *Thermal Spray 2001: New Surface for a New Millennium*, ASM International, ISBN: 0871707373, 2001, p. 281.
- [5] W.J. Lenling, M.F. Smith, J.A. Henfling, in: T.F. Bernecki (Ed.), *Thermal Spray Research and Applications*, ASM International, ISBN: 0-87170-392-0, 1991, p. 227.
- [6] D.A. Stewart, P.H. Shipway, D.G. McCartney, *Surf. Coat. Technol.* 105 (1998) 13.
- [7] W. Lenling, M.F. Smith, J.A. Henfling, *National thermal spray conference*, Long Beach, USA, ISBN: 0871703920, 1990, p. 227.
- [8] P.K. Ghosh, Ram, Neki, *Intern. J. Join. Mater.* 9 (3) (1997) 114.
- [9] V. Stoica, R. Ahmed, T. Itsukaichi, S. Tobe, *Wear* 257 (n11) (December 2004) 1103.
- [10] M. Buchmann, M. Escribano, R. Gadow, G. Burkle, in: C.C. Berndt (Ed.), *Thermal Spray: Surface Engineering via Applied Research*, ASM International, ISBN: 0-87170-680-6, 2002, p. 598.
- [11] P. Ostojic, R. McPherson, *Mater. Forum* 10 (4) (1987) 247.
- [12] V. Stoica, R. Ahmed, S. Tobe, in: C.C. Berndt (Ed.), *Thermal Spray: Surface Engineering via Applied Research*, ASM International, ISBN: 0-87170-680-6, 2002, p. 930.
- [13] Y. Zhu, K. Yukimura, C. Ding, P. Zhang, *Thin Solid Films* 388 (2001) 277.
- [14] B.A. Detering, J.R. Knibloe, T.L. Eddy, in: Thomas F. Bernecki (Ed.), *Thermal Spray Research and Applications, Proceedings of the 3rd National Thermal Spray Conference*, ASM International, ISBN: 0871703920, 1990, p. 27.
- [15] S.J. Kim, J.K. Kim, *J. Nucl. Mater.* 288 (2001) 163.

- [16] A. Yew, M. Jagatia, H. Ensaff, Z.M. Jin, *J. Eng. Med.* 217 (2003) 333 (Proc. Instn Mech. Engrs).
- [17] M.M. Lima, C. Godoy, P.J. Modenesi, J.C. Avelar-Batista, A. Davison, A. Matthews, *Surf. Coat. Technol.* 177–178 (2004) 489.
- [18] E. Lopez Cantera, B.G. Mellor, *Mater. Lett.* 37 (1998) 201.
- [19] H.L. Lovelock, *J. Therm. Spray Technol.* 7 (3) (1998) 357.
- [20] C. Verdon, A. Karimi, J.L. Martin, *Mater. Sci. Eng., A Struct. Mater.: Prop. Microstruct. Process.* 246 (1998) 11.
- [21] H.C. Chen, E. Pfender, J. Heberlein, *Thin Solid Films* 293 (1997) 227.
- [22] R.C. Tucker, *J. Vac. Sci. Technol.* 11 (1974) 725.
- [23] O.C. Brandt, *J. Therm. Spray Technol.* 4 (1995) 147.
- [24] S. Koruda, T.W. Clyne, *Thin Solid Films* 200 (1) (1991) 49.
- [25] ASM Engineered Materials Reference Book, ASM International, 1989, p. 182.
- [26] V. Stoica, R. Ahmed, M. Golshan, S. Tobe, *J. Therm. Spray Technol.* 13 (1) (2004) 93.
- [27] R. Ahmed, S. Stewart, V. Stoica, T. Itsukaichi, *International Thermal Spray Conference (ITSC2004)*, Osaka, Japan, ISBN: 3-87155-792-7, 2004.
- [28] I.M. Hutchings, *Tribology: Friction and Wear of Engineering Materials*, ISBN: 034056184 X, 1992, p. 23.